Available online at www.sciencedirect.com
ScienceDirect
International Journal of Mass Spectrometry 263 (2007) 260–266
International Journal of Mass Spectrometry
www.elsevier.com/locate/ijms

Electronic structure and fragmentation properties of $[Fe_4S_4(SEt)_{4-x}(SSEt)_x]^{2-}$

You-Jun Fu [a,b,1], Julia Laskin [a,b], Lai-Sheng Wang [a,b,*]

[a] *Department of Physics, Washington State University, 2710 University Drive, Richland, WA 99354, USA*
[b] *Fundamental Science Directorate, Pacific Northwest National Laboratory, P.O. Box 999, MSIN K8-88, Richland, WA 99352, USA*

Received 8 January 2007; received in revised form 3 March 2007; accepted 4 March 2007
Available online 12 March 2007

Abstract

A limited exposure of $(n\text{-}Bu_4N)_2[Fe_4S_4(SEt)_4]$ solutions in acetonitrile to air was found to produce a new series of [4Fe–4S] cluster complexes, $[Fe_4S_4(SEt)_{4-x}(SSEt)_x]^{2-}$ ($x = 1$–4), with the original –SEt ligands substituted by –SSEt di-sulfide ligands, which were formed due to partial decomposition of the [4Fe–4S] core in parent $[Fe_4S_4(SEt)_4]^{2-}$. The products were first observed in the experiments with an ESI-ion Trap-TOF mass spectrometer and were further identified using high resolution Fourier transform ion cyclotron resonance (FTICR) mass spectrometer. Photoelectron spectra of the $[Fe_4S_4(SEt)_{4-x}(SSEt)_x]^{2-}$ dianions revealed that the –SSEt coordination induced little change in the electronic structure of the [4Fe–4S] cluster, but the electron binding energies of $[Fe_4S_4(SEt)_{4-x}(SSEt)_x]^{2-}$ increased from 0.52 to 0.73 eV with increase in x from 0 to 4, suggesting a greater electron withdrawing ability of –SSEt than –SEt. In high resolution MS/MS experiments on $[Fe_4S_4(SEt)_3(SSEt)]^{2-/1-}$, clusters with both charge states yielded fragment $[Fe_4S_4(SEt)_3]^-$, suggesting that –SSEt could be lost either as a negatively charged ion $SSEt^-$ from the doubly charged precursor, or as a radical $^\bullet$SSEt from the singly charged species. The biological implication of the interaction between $[Fe_4S_4(SEt)_4]^{2-}$ and O_2 is discussed in comparison to the air exposure of [4Fe–4S] proteins to the air.

Keywords: FTMS; Electrospray ionization source; Tandem mass spectrometry; Photoelectron spectroctroscopy; Fe–S protein

1. Introduction

Iron–sulfur proteins are involved in a wide range of vital biological processes, such as respiration, photosynthesis and nitrogen fixation [1–3]. The active sites of these proteins normally contain iron–sulfur clusters with one to four iron atoms coordinated by inorganic sulfur and incorporated into the protein structure through terminal coordination by cysteine side chains from the proteins. Fe–S proteins are an important class of electron transfer agents and they also have important functions as catalysts and gene transcription regulators [4]. The correlation between the electronic structure of the Fe–S clusters and the functionalities of the proteins has been extensively studied, and it can help the rational design of biomimic catalysts or drugs [5–7]. Experimental investigations have covered both protein samples and synthetic analogues using spectroscopic techniques, such as NMR, ESR, Mossbauer, Raman, etc. [8,9]. All these methods are performed in the condensed phases (solutions or solids).

On the other hand, rapid development of mass spectrometry, in particular, the soft-ionization technique of electrospray ionization (ESI) [10,11], has made it possible to transport intact solution species directly into the gas phase. Tandem mass spectrometry (MS/MS) has been used to analyze metal complex coordination structure in coordination chemistry through ion–molecule reactions [12–14]. Gas phase experiments provide an opportunity to study the intrinsic properties of the Fe–S core without interference resulting from solvent or lattice effects. The technique developed in our laboratory that combines ESI and photoelectron spectroscopy (PES) provides an excellent platform for investigation of the electronic structures of molecules in the gas phase [15]. Using this technique, we have been able to transport a variety of synthetic Fe–S analogue complexes from solution into the gas phase and systematically investigated their electronic properties [16–20]. The PES data provided intrinsic oxidation potentials of the complexes reveal-

* Corresponding author. Tel.: +1 509 376 5050; fax: +1 509 376 6066.
E-mail address: ls.wang@pnl.gov (L.-S. Wang).
[1] Present address: Department of Chemistry, University of Kentucky, Lexington, KY 40506, USA.

1387-3806/$ – see front matter © 2007 Elsevier B.V. All rights reserved.
doi:10.1016/j.ijms.2007.03.001

ing the electrostatic nature of the interactions between the cubane core [4Fe–4S] and the terminal ligands [16,17]. Furthermore, we used collision induced dissociation (CID) to probe the fragmentation properties of the [4Fe–4S] cubane core. We observed symmetric fission of the doubly charged cubane complexes [21–23], $[Fe_4S_4L_4]^{2-} \rightarrow 2[Fe_2S_2L_2]^{-}$, which provided direct experimental evidence for the two-layer spin-coupling model for the [4Fe–4S] cubane core [24–26]. Asymmetric fission channels were also observed for several mixed ligand clusters $[Fe_4S_4L_xL'_{4-x}]^{2-}$ [27]. Novel [2Fe–2S] clusters were created using the asymmetric fission method [28]. Cubane clusters with various oxidation states from $[4Fe–4S]^{-}$ to $[4Fe–4S]^{3+}$ were generated in the form of $[Fe_4S_4L_x]^{-}$ with variable ligand L [29]. In a recent high resolution Fourier transform ion cyclotron resonance (FTICR) mass spectrometric work, MS/MS experiments on mixed ligand complexes $[Fe_4S_4(SEt)_xCl_{4-x}]^{2-}$ $(x = 0–4)$ proved that the coordination environment has a significant influence on the fragmentation properties of [4Fe–4S] clusters [30].

In the current work, we will demonstrate that limited exposure of $[Fe_4S_4(SEt)_4]^{2-}$ solutions to the air results in formation of $[Fe_4S_4(SEt)_{4-x}(SSEt)_x]^{2-}$ species. Photoelectron spectroscopy was used to probe the electronic structure of these novel complexes with disulfide ligands. Fragmentation behavior and stabilities of $[Fe_4S_4(SEt)_3(SSEt)]^{2-/1-}$ were probed using MS/MS experiments in a high resolution FTICR mass spectrometer.

2. Experimental methods

2.1. Sample preparation

All sample preparations were carried out in a dry N_2 glove box. Stock solutions of anions $[Fe_4S_4(SEt)_4]^{2-}$ were prepared by dissolving solid samples of $(n\text{-}Bu_4N)_2[Fe_4S_4(SEt)_4]$ in O_2-free acetonitrile (1×10^{-4} mol/L). Air exposure was carried out in a syringe by letting in an air bubble from the needle and shaking for different periods of time to give a crude control of the degree of air exposure. These solutions were used directly for electrospray in TOF, PES and FTICR experiments.

2.2. TOF-MS and PES spectra

The PES experiments were carried out with a magnetic-bottle PES apparatus equipped with an ESI source, a quadruple ion trap (QIT) and a time-of-flight (TOF) mass spectrometer. Details of the experimental method have been given elsewhere [15–17]. Briefly, solution samples were sprayed from a syringe and the produced anions were guided into the QIT, where they were accumulated for 0.1 s before being extracted into the TOF tube for mass analyses. In the PES spectra, the species of interest were selected and decelerated before being crossed by a laser beam (193 nm) for photodetachment.

2.3. FTICR spectra

The FTICR experiments were performed on a specially designed 6 T instrument at the Pacific Northwest National Laboratory [31]. Ions were generated in a high-transmission external ESI source equipped with an electrodynamic ion funnel, a collision quadrupole, a mass resolving quadrupole and an accumulation quadrupole. The collision quadrupole was operated in the RF only mode for ion focusing.

For surface-induced dissociation (SID) experiments, the resolving quadrupole was operated in its mass-resolving mode with a typical dc offset in the range of 5–10 V. The isotopic envelope of the precursor ion was selected in the resolving quadrupole, and stored in the accumulation quadrupole for 0.5–10 s. Ions were extracted into the electrostatic ion guide, transferred through the ICR cell, and collided with a fluorinated self-assembled monolayer (FSAM) surface at normal incidence [31–34]. The collision energy was calculated from the potential difference between the offset of the accumulation quadrupole and the surface.

In CID experiments, the resolving quadruple was operated in an RF only mode. All ions generated in the ESI source were transferred into the ICR cell and captured using gated trapping. In MS/MS experiments, all unwanted ions were ejected by applying a stored waveform inverse Fourier transform (SWIFT) excitation [35,36]. Sustained off-resonance irradiation (SORI)-CID experiments [37] were performed on the isolated single isotope peak or an isotopic envelope of the ion of interest. Collision gas (Ar or O_2) was introduced into the cell using a pulsed valve. The isolated precursor ions were radially excited slightly off resonance for 40 ms with maximum collision energies in the range of 0.5–1.7 eV by changing the peak-to-peak voltage applied to the excitation plates. After 10 s pumping delay, ions in the cell were excited for detection by broadband chirp excitation. The maximum kinetic energy (peak–peak) achieved in SORI-CID was calculated as previously reported [31–35].

2.4. UV–vis absorption spectra

Solutions with different degree of air-exposure prepared in a syringe, as described above, were diluted directly into a well-sealed quartz cuvette to about 10^{-5} to 10^{-6} mol/L using O_2-free solvent in a glove box. The UV–vis absorption spectra were measured using a commercial UV–vis spectrophotometer (Varian Analytical Instruments).

3. Results

3.1. ESI-TOF mass spectra

Fe–S cluster complexes are known to be extremely air-sensitive. All relevant experiments are usually carried out under inert gas atmosphere with purged solvent to remove the residual air. A typical TOF mass spectrum for a clean acetonitrile solution of $(Bu_4N)_2[Fe_4S_4(SEt)_4]$ is shown in Fig. 1a with only one peak at *m/z* 298, corresponding to the parent cubane core. However, when an unpurged acetonitrile solvent was accidentally used to dissolve $(Bu_4N)_2[Fe_4S_4(SEt)_4]$, a series of unexpected peaks was observed in addition to the precursor ion peak. Shown in Fig. 1b is a spectrum taken using a sample prepared by controlled air-exposure. Exposure of $(Bu_4N)_2[Fe_4S_4(SEt)_4]$ to the laboratory air yields four new peaks at *m/z* 314, 330, 346 and 362 with

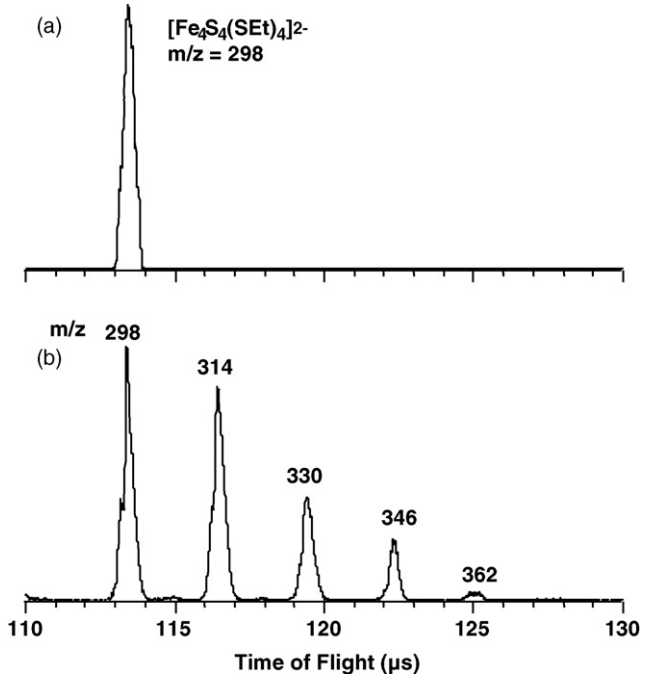

Fig. 1. (a) TOF mass spectrum of $Fe_4S_4(SEt)_4^{2-}$ from a clean $(n\text{-}Bu_4N)_2[Fe_4S_4(SEt)_4]$ solution in N_2-purged acetonitrile. (b) Typical TOF mass spectrum from an solution of $(n\text{-}Bu_4N)_2[Fe_4S_4(SEt)_4]$ in acetonitrile after some degree of air-exposure.

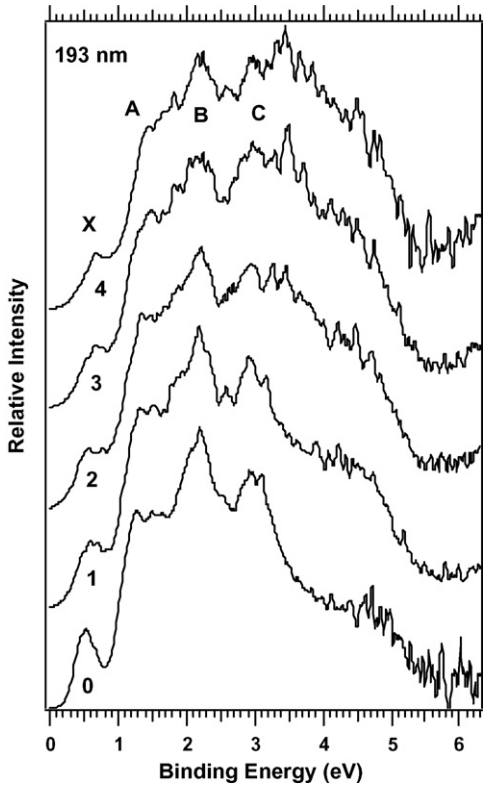

Fig. 2. PES Spectra of $[Fe_4S_4(SEt)_{4-x}(SSEt)_x]^{2-}$ at 193 nm ($x = 0$–4).

decreasing intensity. The new peaks are separated by 16 u. Since these species are all doubly charged anions, the mass difference for the peaks is 32 u, which could be due to either addition of an O_2 molecule or addition of an S atom to the precursor ion.

3.2. PES spectra

Fig. 2 displays 193 nm PES spectra of the newly observed species (Fig. 1b) in comparison to the PES spectrum of the precursor dianion, $[Fe_4S_4(SEt)_4]^{2-}$, which has been reported previously [16]. The PES spectra of the new species exhibited similar spectral patterns as the parent cubane complex. But the electron binding energies, as measured from the vertical detachment energy (VDE) of the first band (X), increased from 0.52 for the parent to 0.58, 0.67, 0.70 and 0.73 eV, for $m/z = 314$, 330, 346 and 362 species (labeled as 1–4 in Fig. 2), respectively. The obvious spectral cutoffs at the higher binding energy side were due to the existence of the repulsive coulomb barrier (RCB), characteristic of PES for multiply charged anions [38–40]. The similarity between PES spectra of all the species clearly suggests that the [4Fe–4S] cubane core is intact in all the new species.

3.3. FTICR mass spectra and the identity of the new mass peaks

To determine if the new species were due to the addition of an O_2 molecule or an S atom, we performed high resolution mass spectrometry using FTICR mass spectrometry. Fig. 3 displays a FTICR mass spectrum taken directly from spraying an air-exposed sample of $(Bu_4N)_2[Fe_4S_4(SEt)_4]$. The peak at m/z 298 is the parent complex $[Fe_4S_4(SEt)_4]^{2-}$, while the peak at m/z 596 is the singly charged $[Fe_4S_4(SEt)_4]^-$ ion resulting from collisional electron loss from the parent dianion [30]. A relatively abundant peak at m/z 314 was also observed. The inset in Fig. 3 shows the isotopic distribution of the parent $[Fe_4S_4(SEt)_3(SSEt)]^{2-}$ dianion: the 0.5 difference in m/z between the neighboring peaks confirms its doubly charged character. The exact isotopic m/z difference between the m/z 314 peak and the parent was measured as 15.98565, corresponding to a mass difference of 31.97130 amu. This mass difference agrees well with the mass of an S atom (31.97207 amu), thus excluding the possibility of O_2 addition (mass of O_2: 31.98983 amu).

To determine the mode of binding of the S atom in the new species, we carried out collision-induced dissociation (CID) experiments. The SWIFT technique was used to isolate a single

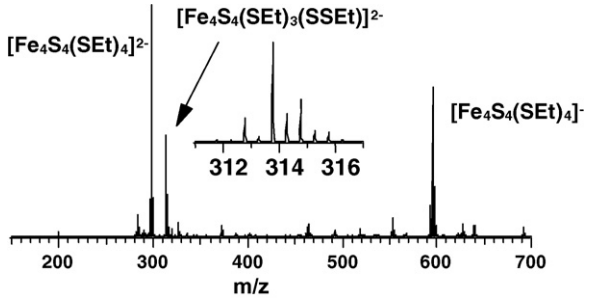

Fig. 3. High-resolution mass spectrum from an solution of $(n\text{-}Bu_4N)_2[Fe_4S_4(SEt)_4]$ in acetonitrile after air-exposure. The inset displays the measured isotopic distribution of the $[Fe_4S_4(SEt)_3(SSEt)]^{2-}$ dianion.

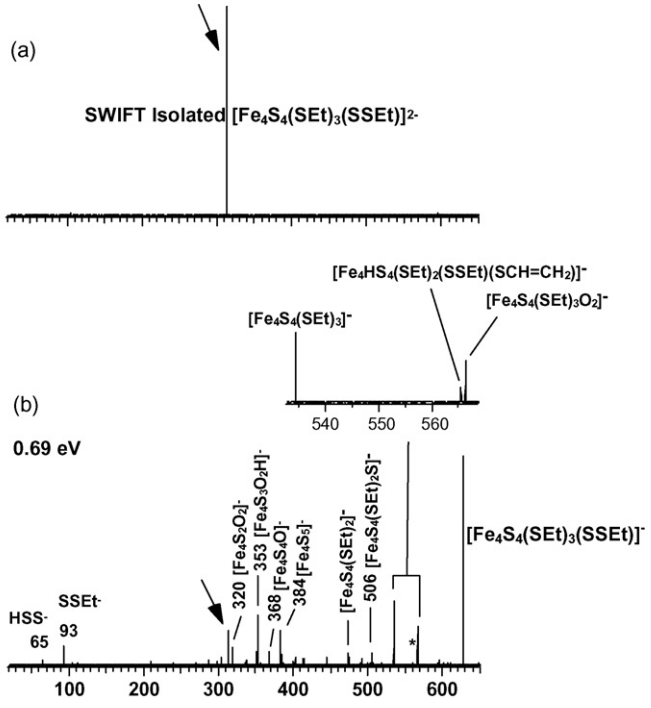

Fig. 4. CID results of $[Fe_4S_4(SEt)_3(SSEt)]^{2-}$. (a) SWIFT isolated $[Fe_4S_4(SEt)_3(SSEt)]^{2-}$ and (b) CID result at collision energy 0.69 eV. Identification: 65.0, HSS^-; 93.0, $SSEt^-$; 313.8, $[Fe_4S_4(SEt)_3(SSEt)]^{2-}$; 351.7, $[Fe_4S_3O_2]^-$; 352.7, $[Fe_4S_3O_2H]^-$; 367.6, $[Fe_4S_4O]^-$; 383.6, $[Fe_4S_5]^-$; 473.7, $[Fe_4S_4(SEt)_2]^-$; 505.6, $[Fe_4S_4(SEt)(SSEt)]^-$; 534.7, $[Fe_4S_4SEt_3]^-$; 566.7, $[Fe_4S_4(SEt)_3O_2]^-$; 627.7, $[Fe_4S_4(SEt)_3(SSEt)]^-$.

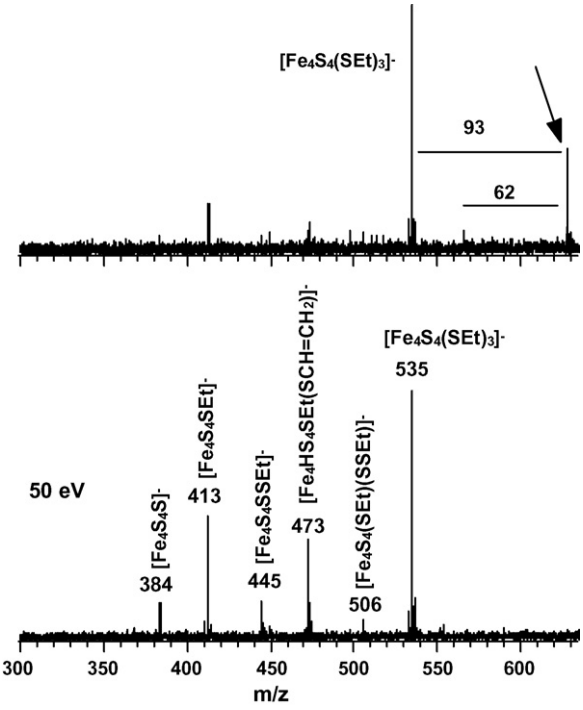

Fig. 5. SID of $[Fe_4S_4(SEt)_3(SSEt)]^-$ at 30 eV (top), 50 eV (bottom). Identification and relative abundance are listed in Table 1.

isotopic peak or the whole envelope of the *m/z* 314 species for CID (see Fig. 4a). Fig. 4b shows SORI-CID spectrum of the isolated isotopomer at collision energy of 0.69 eV. Loss of $[SSEt]^-$ from the precursor dianion resulting in formation of two complementary ions at *m/z* 535 ($[Fe_4S_4(SEt)_3]^-$) and *m/z* 93 ($[SSEt]^-$) suggests that additional sulfur in the $[Fe_4S_4(SEt)_4 + S]^{2-}$ species is not attached directly to the [4Fe–4S] core but rather inserted into a new disulfide ligand –SSEt. It follows that the new species at *m/z* 314 is $[Fe_4S_4(SEt)_3(SSEt)]^{2-}$. Similar results were obtained for other members of the series shown in Fig. 1b suggesting that the new series of species have a general formula of $[Fe_4S_4(SEt)_{4-x}(SSEt)_x]^{2-}$, $x = 1$–4.

The identification of the –SSEt coordination was also verified using SID experiments on the singly charged $[Fe_4S_4(SEt)_3(SSEt)]^-$ (*m/z* 628) species, at collision energies of 30, 50, 70 and 100 eV. Shown in Fig. 5 are spectra taken at 30 and 50 eV. The peak at *m/z* 535 with a 93 u difference from the parent $[Fe_4S_4(SEt)_3(SSEt)]^-$ (*m/z* 628) is significant indicating loss of a $^{\bullet}$SSEt ligand (Fig. 5a). Additional peak assignments are listed in Table 1.

In CID experiments on the singly charged $[Fe_4S_4(SEt)_3(SSEt)]^-$ ion, the whole isotopic envelope of $[Fe_4S_4(SEt)_3(SSEt)]^-$ was isolated (Fig. 6a) to obtain its MS/MS spectrum at different collision energies (Fig. 6b). Again $[Fe_4S_4(SEt)_3]^-$ was observed, indicating loss of $^{\bullet}$SSEt, consistent with the SID results.

3.4. UV–vis absorption spectra

It was unexpected that the limited air-exposure produced the new species with $SSEt^-$ coordination instead of instant precipitation of iron oxides, or sulfides. To investigate the influence of air exposure on the solution properties, UV–vis absorption spectra of the samples with different degrees of air-exposure were measured (Fig. 7). With no air exposure a well-defined absorption curve with the typical absorption of $[Fe_4S_4(SEt)_4]^{2-}$ at 304 and 417 nm was obtained. With the increase of air exposure, the absorption intensities of both peaks

Table 1
Relative abundance of the fragments from SID experiments

SID energy (eV)	$[Fe_4S_4(SEt)_3(SSEt)]^-$, 627.7	$[Fe_4S_4(SEt)_3]^-$ 534.7	$[Fe_4HS_4SEt(SCH{=}CH_2)]^-$, 472.7	$[Fe_4S_4SSEt]^-$, 444.6	$[Fe_4S_4SEt]^-$, 412.7	$[Fe_4S_4S]^-$, 383.6
30	42.7	100	9.6		20.1	
50		100	40.3	15.5	50.3	14.5
70		27.5	27.4	32.9	100	55.9
100		13.3	12.4	33.5	45.3	100

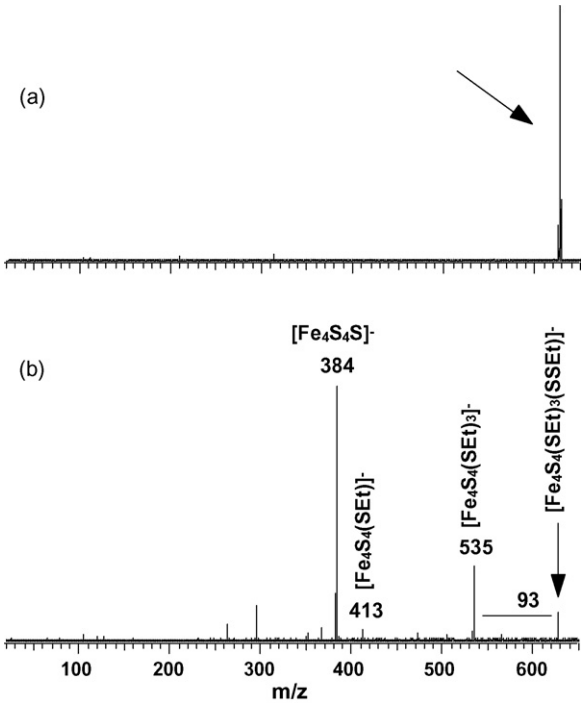

Fig. 6. CID results of $[Fe_4S_4(SEt)_3(SSEt)]^-$: (a) SWIFT isolated isotopic envelope of $[Fe_4S_4(SEt)_3(SSEt)]^-$ and (b) CID of $[Fe_4S_4(SEt)_3(SSEt)]^-$ at 2.0 eV. Identification: 383.6, $[Fe_4S_5]^-$; 412.7, $[Fe_4S_4(SEt)]^-$; 534.7, $[Fe_4S_4(SEt)_3]^-$; 627.7, $[Fe_4S_4(SEt)_3(SSEt)]^-$.

decreased and at the same time a new broad absorption feature appeared in the range of 500–700 nm initially. Although this new absorption feature was broad and weak, the occurrence of an isosbestic point at about 500 nm indicated the formation of new species. The new absorption band was tentatively assigned to the –SSEt-coordinated cubanes. With further air exposure, both the absorption bands due to the parent and the –SSEt-coordinated cubanes disappeared, suggesting that the cubanes were completely decomposed. The final result was a red-brown precipitate, which should be a complex mixture of oxide and sulfide of Fe(III) and Fe(II).

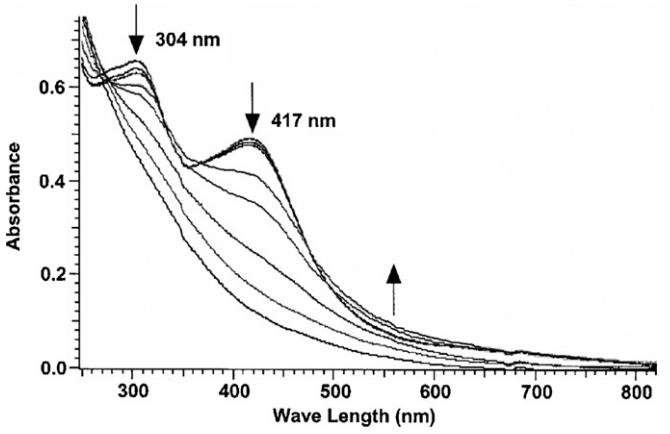

Fig. 7. UV–vis absorption spectra of $(n\text{-}Bu_4N)_2[Fe_4S_4(SEt)_4]$ with different degree of air exposure. Arrows ↓ and ↑ indicate decreasing and increasing absorbance intensity, respectively, with increasing air exposure.

4. Discussion

4.1. Electronic structure

The similarity of the PES spectra of $[Fe_4S_4(SEt)_{4-x}(SSEt)_x]^{2-}$ from $x = 0$ to 4 (Fig. 2) suggests that the coordination of the –SSEt ligand does not have a significant effect on the electronic structure of the [4Fe–4S] cluster core. As reported previously for the PES spectrum of $[Fe_4S_4(SEt)_4]^{2-}$ [16], feature X is assigned to the highest occupied molecular orbital (HOMO) of the cubane with two degenerate minority 3d electrons and feature A is assigned to HOMO-1, which is mainly from the bridging sulfur ligand [16,17]. Features B and C are assigned to the –SEt and –SSEt ligand orbitals, consistent with the fact that their binding energies do not change with x. The most significant change in the PES spectra was the VDE of the first band (X), which increased from 0.52 eV for $x = 0$–0.73 eV for $x = 4$. This observation suggests that the –SSEt ligand possesses stronger electron withdrawing ability than the –SEt ligand.

4.2. Fragmentation properties

The [4Fe–4S] cubane core consists of two antiferromagnetically coupled [2Fe–2S] layers. This structure results in symmetric fission of the doubly charged precursor anions upon collisional activation [20–22,26–28]. Our most recent work on mixed ligand systems $[Fe_4S_4(SEt)_{4-x}Cl_x]^{2-}$ showed that Cl substitution has a significant effect on the fragmentation behavior of the cubanes. For example, the propensity of the fission channel increases with the number of Cl^- coordination [30]. In the current MS/MS (CID and SID) experiments, all the observed fragments are singly charged species reflecting the great tendency for the two charges of the dianions to separate due to the strong intramolecular Coulomb repulsion and the relatively low electron binding energies. This is in general very similar to the previously reported results for $[Fe_4S_4(SEt)_{4-x}Cl_x]^{2-}$ [28,30].

Similar to $[Fe_4S_4(SEt)_4]^{2-}$, collision-induced electron detachment in $[Fe_4S_4(SEt)_3(SSEt)]^{2-}$ is the dominating channel, giving rise to the peak at m/z 628 (Fig. 4):

$$[Fe_4S_4(SEt)_3(SSEt)]^{2-} \quad (m/z \quad 314)$$
$$\rightarrow [Fe_4S_4(SEt)_3(SSEt)]^- \quad (m/z \quad 628) + e \qquad (1)$$

However, different from $[Fe_4S_4(SEt)_4]^{2-}$, which exhibited basically only the electron detachment channel, $[Fe_4S_4(SEt)_3(SSEt)]^{2-}$ gave abundant other fragmentation channels (Fig. 4). Although in minor abundances, neutral losses of m/z 94 (HSSEt) and 62 (HSEt) were observed in Fig. 4(b) (labeled with *) which also shows abundant negatively charged ligand loss –SSEt resulting in the peaks at m/z 93 ($SSEt^-$) and 535 ($[Fe_4S_4(SEt)_3]^-$),

$$[Fe_4S_4(SEt)_3(SSEt)]^{2-} \rightarrow [Fe_4S_4(SEt)_3]^- + SSEt^- \qquad (2)$$

Differently, in the case of $[Fe_4S_4(SEt)_4]^{2-}$, we never saw any loss of –SEt (61) or formation of $[Fe_4S_4(SEt)_3]^-$ (535), while in the $[Fe_4S_4(SEt)_{4-x}Cl_x]^{2-}$ series, it is only when x is greater than 2 that the loss of Cl^- showed up significantly [30]. This major

fragmentation channel represented by Eq. (2) reflects a weaker covalent interaction of the [4Fe–4S] core with the –SSEt ligand than with the –SEt ligand.

The neutral loss of *m/z* 62 (HSEt) shown in Fig. 4b (labeled with *) and Fig. 5a at the position of *m/z* 566, *m/z* 62 different from the parent $[Fe_4S_4(SEt)_3(SSEt)]^-$. Due to the co-existence of SSEt and SEt ligand it is interesting that this neutral loss can be produced in two ways represented by Eqs. (3) and (4):

$$[Fe_4S_4(SEt)_3(SSEt)]^{2-} \rightarrow [Fe_4HS_4(SEt)_2(SSCH{=}CH_2)]^- + HSEt \quad (3)$$

$$[Fe_4S_4(SEt)_3(SSEt)]^{2-} \rightarrow [Fe_4HS_4(SEt)(SCH{=}CH_2)(SSEt)]^- + HSEt \quad (4)$$

Most likely the peak at *m/z* 566 is a mixture of $[Fe_4HS_4(SEt)(SCH{=}CH_2)(SSEt)]^-$ and $[Fe_4HS_4(SEt)_2(SSCH{=}CH_2)]^-$ because both peaks at *m/z* 506 ($[Fe_4S_4(SEt)(SSEt)]^-$) and 474 ($[Fe_4S_4(SEt)_2]^-$) corresponding to the neutral loss of $HSSCH{=}CH_2$ (92), and $HSCH{=}CH_2$ (60) according to reactions (5) and (6), respectively, appear in the SORI-CID spectrum (Fig. 4b).

$$[Fe_4HS_4(SEt)(SCH{=}CH_2)(SSEt)]^- \rightarrow [Fe_4HS_4(SEt)(SSEt)]^- + HSCH{=}CH_2 \quad (5)$$

$$[Fe_4HS_4(SEt)_2(SSCH{=}CH_2)]^- \rightarrow [Fe_4HS_4(SEt)_2]^- + HSSCH{=}CH_2 \quad (6)$$

Channels (3)–(6) are analogous to the neutral loss of HSEt, and $HSCH{=}CH_2$ in the fragmentation of $[Fe_4S_4(SEt)_4]^-$ [30].

Both CID and SID (Figs. 5 and 6) of the singly charged $[Fe_4S_4(SEt)_3(SSEt)]^-$ ion resulted in formation of an abundant $[Fe_4S_4(SEt)_3]^-$ fragment at *m/z* 535 suggesting radical loss of $^{\bullet}SSEt$ from the precursor ion:

$$[Fe_4S_4(SEt)_3(SSEt)]^- \rightarrow [Fe_4S_4(SEt)_3]^- + {}^{\bullet}SSEt \quad (7)$$

It should be noted that the corresponding channel was not observed for $[Fe_4S_4(SEt)_4]^-$ which showed only neutral loss of HSEt (62) to form hydrogen coordinated species $[Fe_4HS_4(SEt)_2(SCH{=}CH_2)]^-$.

4.3. The implication of $[Fe_4S_4(SEt)_{4-x}(SSEt)_x]^{2-}$ formation in solution with O_2 exposure

High-resolution mass spectrometry allowed us to confirm the formation of a series of sulfur insertion complexes, $[Fe_4S_4(SEt)_{4-x}(SSEt)_x]^{2-}$, following limited exposure of solutions containing $[Fe_4S_4(SEt)_4]^{2-}$ to laboratory air. Becuase the original sample contained only $[Fe_4S_4(SEt)_4]^{2-}$, formation of the –SSEt ligand suggests that inorganic sulfur is released into the solution following its exposure to air. The additional sulfur is most likely released as a result of partial destruction of the [4Fe–4S] cluster complexes. The new ligand is formed following solution-phase decomposition of some precursor cubane molecules,

$$S + SEt^- \rightarrow SSEt^- \quad (8)$$

Substitution reaction results in formation of four additional species, with $x = 0 - 4$ in Eq. (9),

$$[Fe_4S_4(SEt)_4]^{2-} + xSSEt^- \rightarrow [Fe_4S_4(SEt)_{4-x}(SSEt)_x]^{2-} + xSEt^- \quad (9)$$

From the UV–vis absorption measurements, a new band in the range from 500 to 700 nm was observed. Although $[Fe_2S_2(SEt)_4]^{2-}$ absorbs in the range from 500 to 700 nm, it can be excluded since our mass spectra showed neither this doubly charged species at *m/z* 210 nor its electron detached product $[Fe_2S_2(SEt)_4]^-$ at *m/z* 420. As previously reported on the interaction of O_2 with various Fe(II) proteins and their analogues, the charge transfer energy from O_2^- to Fe(III) corresponds to an absorption band in the range 500–700 nm [3]. In the case of $[Fe_4S_4(SEt)_{4-x}(SSEt)_x]^{2-}$, it is most possible that the charge transfer from –SSEt to Fe(III) is strong enough to result in absorption in this range although the intensity is much lower.

Although the sensitivity of Fe–S clusters to air causes much problem in the laboratory experiments, nature makes very good use of it in the function of Fe–S proteins. For example, aconitase, a [4Fe–4S] enzyme catalyzing the inter-conversion between citric and iso-citric acid, would react with O_2 and its [4Fe–4S] active center would lose one iron corner to form [3Fe–4S] cluster inactivating the protein [41,42]. Another example is the interaction of fumarate and nitrate reduction (FNR) with O_2, which would change the protein into its [2Fe–2S] form and make it lose its DNA binding ability [42–46]. In fact, the UV–vis curves we observed here are very similar to those reported in the interaction of O_2 with FNR where the new band was assigned to the formation of [2Fe–2S] clusters [46–48]. The detailed mechanism of the interaction between O_2 and Fe–S proteins is still not well understood. However, from the current results we know that S–S bond can actually form with ease through the partial destruction of Fe–S cluster when the sample was exposed to air. Because of the similarity between the –SEt group and –Cysteine residue the synthetic Fe–S cluster $[Fe_4S_4(SEt)_4]^{2-}$ provides a good model to study the interaction of O_2 with Fe–S proteins in which the [4Fe–4S] cluster has four cysteine residuals as the terminal ligands. We do not know if it has any biological implication, but this S–S ligand coordination seems to be one of the intermediates, or side product, in the interaction of O_2 with Fe–S protein. The fragmentation experiments showed that the Fe–SSEt bond is weaker and more ionic than the Fe–SEt bond. In the protein systems, it is possible that the intermediate Fe–SSCys coordination, which is easier to dissociate, would decrease the energy barrier for further reaction to happen. Recent mass spectrometric results showed that SSCys ligand does form in Fe–S protein systems in the presence of air [49–52]. In earlier experiments, it was actually always a problem in biological analysis to determine the right Fe/S ratio and right number of Fe and/or S in the proteins. Because some degree of air exposure can readily occur during the protein purification, partial destruction of the Fe–S

cluster and the resulting formation of S–S bond in the protein system is definitely one of the results which would change the Fe/S ratio in an elusive way.

5. Conclusions

Interaction between O_2 and $[Fe_4S_4(SEt)_4]^{2-}$ in solution was observed to cause partial decomposition of the [4Fe–4S] cluster, releasing inorganic sulfur and SEt ligands. The newly formed SSEt ligand can substitute sequentially the SEt ligand in the parent to form a new series of species, $[Fe_4S_4(SEt)_{4-x}(SSEt)_x]^{2-}$. Photoelectron spectroscopy revealed that the SSEt ligand coordination has no significant influence on the electronic structure of the [4Fe–4S] cluster, but results in increase in the electron binding energy suggesting greater electron withdrawing ability of –SSEt as compared to SEt. High resolution MS/MS measurements revealed that $[Fe_4S_4(SEt)_{4-x}(SSEt)_x]^{2-}$ did not undergo symmetric fission, but rather exhibited significant loss of the –SSEt ligand, indicating that the interaction of Fe–SSEt is weaker than that of Fe–SEt. The interaction of $[Fe_4S_4(SEt)_4]^{2-}$ with O_2 in solution is expected to be similar to that of 4Fe–4S proteins implying that S–S bond formation is most possibly one of the intermediates in the interaction of O_2 with Fe–S proteins.

Acknowledgments

This work was supported by the National Institutes of Health (GM-63555 to L.S.W.) and the Chemical Science Division of the Office of Basic Energy Sciences, U.S. Department of Energy (to J.L.). The experimental work was performed at the W.R. Wiley Environmental Molecular Sciences Laboratory, a national scientific user facility sponsored by DOE's Office of Biological and Environmental Research and located at Pacific Northwest National Laboratory, which is operated for DOE by Battelle.

References

[1] W. Lovenberg (Ed.), Iron–Sulfur Proteins, vols. I and II, Academic Press, New York, 1973.
[2] T.G. Spiro (Ed.), Iron–Sulfur Proteins, Wiley-Interscience, New York, 1982.
[3] R. Cammack, Adv. Inorg. Chem. 38 (1993) 281.
[4] H. Beinert, R.H. Holm, E. Munck, Science 277 (1997) 653.
[5] D.H. Flint, R.M. Allen, Chem. Rev. 96 (1996) 2315–2334.
[6] A. Lombardi, C.M. Summa, S. Geremia, L. Randaccio, V. Pavone, W.F. DeGrado, PNAS 97 (2000) 6298–6305.
[7] S.E. Mulholland, B.R. Gibney, F. Rabanal, P.L. Dutton, J. Am. Chem. Soc. 120 (1998) 10296–10302.
[8] A.G. Sykes, R. Cammack (Eds.), Adv. Inorg. Chem., vol. 47, Academic Press, New York, 1999.
[9] P.V. Rao, R.H. Holm, Chem. Rev. 104 (2004) 527–559.
[10] J.B. Fenn, M. Mann, C.K. Meng, S.F. Wong, C.M. Whitehouse, Science 246 (1989) 64.
[11] J.B. Fenn, J. Am. Soc. Mass Spectrom. 4 (1993) 524–535.
[12] L. Gianelli, V. Amendola, L. Fabbrizzi, P. Pallavicini, G.G. Mellerio, Rapid Commun. Mass Spectrom. 15 (2001) 2347–2353.
[13] R.W. Vachet, J.A.R. Hartman, J.W. Gertner, J.H. Callahan, Int. J. Mass Spectrom. 204 (2001) 101–112.
[14] M.Y. Combariza, A.M. Fahey, A. Milshteyn, R.W. Vachet, Int. J. Mass Spectrom. 244 (2005) 109–124.
[15] L.S. Wang, C.F. Ding, X.B. Wang, S.E. Barlow, Rev. Sci. Instrum. 70 (1999) 1957.
[16] X.B. Wang, S. Niu, X. Yang, S.K. Ibrahim, C.J. Pickett, T. Ichiye, L.S. Wang, J. Am. Chem. Soc. 125 (2003) 14072–14081.
[17] Y.J. Fu, X. Yang, X.B. Wang, L.S. Wang, Inorg. Chem. 43 (2004) 3647–3655.
[18] X. Yang, S. Niu, T. Ichiye, L.S. Wang, J. Am. Chem. Soc. 126 (2004) 15790–15794.
[19] X. Yang, X.B. Wang, Y.J. Fu, L.S. Wang, J. Phys. Chem. A 107 (2003) 1703.
[20] X. Yang, X.B. Wang, Y.J. Fu, L.S. Wang, in: J. Laskin, C. Lifshitz (Eds.), Principles Mass Spectrometry Applied to Biomolecules, Wiley, New Jersey, 2006, pp. 63–117.
[21] X. Yang, X.B. Wang, S.Q. Niu, C.J. Pickett, T. Ichiye, L.S. Wang, Phys. Rev. Lett. 89 (2002) 163401.
[22] X. Yang, X.-B. Wang, L.-S. Wang, Int. J. Mass Spectrom. 228 (2003) 797.
[23] S. Niu, X.-B. Wang, X. Yang, L.-S. Wang, T. Ichiye, J. Phys. Chem. A 108 (2004) 6750.
[24] L. Noodleman, E.J. Baerends, J. Am. Chem. Soc. 106 (1984) 2316.
[25] L. Noodleman, D.A. Case, Adv. Inorg. Chem. 38 (1992) 423.
[26] L. Noodleman, C.Y. Peng, D.A. Case, J.M. Mouesca, Coord. Chem. Rev. 144 (1995) 199.
[27] Y.-J. Fu, X. Yang, X.-B. Wang, L.-S. Wang, J. Phys. Chem. A. 109 (2005) 1815.
[28] Y.-J. Fu, S.-Q. Niu, T. Ichiye, L.-S. Wang, Inorg. Chem. 44 (2005) 1202.
[29] H.-J. Zhai, X. Yang, Y.-J. Fu, X.-B. Wang, L.-S. Wang, J. Am. Chem. Soc. 126 (2004) 8413–8420.
[30] Y.-J. Fu, J. Laskin, L.S. Wang, Int. J. Mass Spectrom. 255/256 (2006) 102–110.
[31] J. Laskin, E.V. Denisov, A.K. Shukla, S.E. Barlow, J.H. Futrell, Anal. Chem. 74 (2002) 3255.
[32] J. Laskin, J.H. Futrell, Mass Spectrom. Rev. 22 (2003) 158.
[33] J. Laskin, E. Denisov, J. Futrell, J. Am. Chem. Soc. 122 (2000) 9703.
[34] J. Laskin, M. Byrd, J. Futrell, Int. J. Mass Spectrom. 195 (2000) 285.
[35] L.J. de Koning, N.M.M. Nibbering, S.L. van Orden, F.H. Laukien, Int. J. Mass Spectrom. Ion Processes 165/166 (1997) 209.
[36] G. Kruppa, P.D. Schnier, K. Tabei, S.L. van Orden, M.M. Siegel, Anal. Chem. 74 (2002) 3877.
[37] J.W. Gauthier, T.R. Trautman, D.B. Jacobson, Anal. Chim. Acta 246 (1991) 211.
[38] X.B. Wang, C.F. Ding, L.S. Wang, Phys. Rev. Lett. (1998) 3351–3354.
[39] L.S. Wang, C.F. Ding, X.B. Wang, J.B. Nicholas, Phys. Rev. Lett. 81 (1998) 2667–2670.
[40] L.S. Wang, X.B. Wang, J. Phys. Chem. A 104 (2000) 1978–1990.
[41] E. Kimura, M. Kodama, R. Machida, K. Ishizu, Inorg. Chem. 21 (1982) 595, 602.
[42] H. Beinert, M.C. Kennedy, C.D. Stout, Chem. Rev. (1996) 2335–2373.
[43] C.E. Bauer, S. Elsen, T.H. Bird, Annu. Rev. Microbiol. 53 (1999) 495–523.
[44] B.A. Lazazzera, H. Beinert, N. Khoroshilova, M.C. Kennedy, P.J. Kiley, J. Biol. Chem. 271 (1996) 2762–2768.
[45] N. Khoroshilova, C. Popescu, E. Munck, H. Beinert, P.J. Killey, PNAS 94 (1997) 6087–6092.
[46] P.J. Kiley, H. Beinert, Curr. Opin. Microbiol. 6 (2003) 181–185.
[47] P.A. Jordan, A.J. Thomson, E.T. Ralph, J.R. Guest, J. Green, FEBS Lett. 416 (1997) 349–352.
[48] H. Hernadez, K.S. Hewitson, P. Roach, N.M. Shaw, J.E. Baldwin, C.V. Robinson, Anal. Chem. 73 (2001) 4154–4161.
[49] P.K. Taylor, D.M. Kurtz Jr., I.J. Amster, Int. J. Mass Spectrom. 210/211 (2001) 651–663.
[50] K.A. Johnson, M.F.J.M. Verhagen, M.W.W. Adams, I.J. Amster, Int. J. Mass Spectrom. 204 (2001) 77–85.
[51] K.A. Johnson, B.A. Shira, J.L. Anderson, I.J. Amster, Anal. Chem. 73 (2001) 803–808.
[52] Q.P. Lei, X. Cui, D.M. Kurtz Jr., I.J. Amster, Anal. Chem. 70 (1998) 1838–1846.